

# Ambient temperature and free stream turbulence effects on the thermal transient anemometer

J F Foss, J A Peabody, M J Norconk and A R Lawrenz

Turbulent Shear Flows Laboratory, Michigan State University, A-138 Engineering Research Complex, E Lansing, MI 48823, USA

Received 13 June 2006, in final form 20 July 2006

Published 17 August 2006

Online at [stacks.iop.org/MST/17/2519](http://stacks.iop.org/MST/17/2519)

## Abstract

The thermal transient anemometer is a measurement device to obtain area average values of temperature and velocity. Its development was motivated by HVAC (heating, ventilation and air conditioning) and cooling-air circuit automotive development efforts. Analytic considerations, which address utilizing room temperature velocity calibration data in applications with elevated ambient temperatures, have been evaluated and supported by direct experiments. Free stream turbulence levels, as expected for the intended applications, have also been shown to have no effect on the velocity calibrations.

**Keywords:** spatially averaged velocity and temperature

(Some figures in this article are in colour only in the electronic version)

## Nomenclature

$A_c$	cross-sectional area of wire (equation (3))	$T_w$	average temperature of sensor wire along length (equation (2))
$A_p$	perimetral area of wire (equation (4))	$T_{hot}$	maximum temperature of sensor wire (equation (7b))
$c$	specific heat of wire (equation (2))	$T_{Low}$	lowest temperature of sensor wire that is used in the exponential decay curve (equation (7c))
$d$	wire diameter (equation (6))	$T_f$	film temperature of air around sensor wire (equation (7a))
$h$	convective heat transfer coefficient (equation (4))	$\tilde{u}$	velocity fluctuation intensity
$k_f$	thermal conductivity of air at film temperature (equation (6))	$V$	flow velocity (equation (8))
$k_w$	thermal conductivity of wire (equation (3))	$x$	distance along length of wire (equation (3))
$L$	wire length (equation (3))	$\alpha$	temperature coefficient of resistance (equation (1))
$m$	mass of wire (equation (2))	$\nu_f$	kinematic viscosity at film temperature (equation (8))
$p_{atm}$	atmospheric static pressure (equation (12))	$\tau$	time constant of exponential decay (equation (10a))
$p_{Pitot}$	stagnation pressure from Pitot tube		
$p_{tap}$	static pressure of calibration flow (equation (12))		
$\dot{Q}$	rate of thermal energy loss by wire (equation (2))		
$R$	electrical resistance (equation (1))		
$T_{a]measurement}$	temperature of ambient fluid during measurement		
$T_{a]calibration}$	temperature of ambient fluid during calibration		

## 1. Introduction

The thermal transient anemometer<sup>1</sup> (TTA) was introduced by Foss *et al* [1]. This measurement tool provides area averaged

<sup>1</sup> US Patent No 7,051,599, thermal transient anemometer having sensing cell assembly, 30 May 2006.



(a)



(b)

**Figure 1.** A TTA cell and frame. (a) A single TTA cell; (b) a  $4 \times 5$  frame for an off-road vehicle.

values of the velocity and temperature for a ‘cell’. The complete area of interest, for example a heat exchanger or the area of a conduit, would be surveyed by a ‘frame’ that would contain a number of cells. In a typical application, a frame would provide  $N \times M$  cells where  $16 \lesssim N \times M \leq 32$ .

Figure 1(a) presents a freestanding cell; figure 1(b) shows a  $4 \times 5$  cell that was prepared for the evaluation of an off-highway vehicle’s radiator. The multi-X patterns of figure 1 identify the technique to recover an ‘area average’. The sensor wire is a tungsten alloy with typical diameters in the range of  $0.1 \lesssim d(\text{mm}) \lesssim 0.2$ . The sensor wires are tethered in Teflon plugs and they are stretched taut to avoid centre point contact when they expand as a result of an elevated temperature.

The control electronics unit (see Foss *et al* [1]) is first used to determine the ambient temperature of the flowing air through the cell. This is accomplished by reading the sensor’s resistance ( $R$ ) and utilizing the temperature coefficient of resistance ( $\alpha$ ) as

$$R(T) = R(T_o)\{1 + \alpha(T - T_o)\}. \quad (1)$$

It has been found to be important to carry out a calibration process for  $\alpha$  since the particular sensor wire will have some alloy content and an annealing history that preclude the use of a tabulated  $\alpha$  value.

The velocity magnitude is obtained by (i) elevating the sensor wire temperature with a heating current ( $I^2R$ ) to a temperature that is safely below the metal’s oxidation temperature ( $\approx 300^\circ\text{C}$ ), (ii) impulsively reducing the heating current to zero and (iii) measuring the falling resistance  $R(t)$ , as the wire cools toward its ambient temperature. The analysis and data of Foss *et al* [1] and that presented below will show that an exponential decay is both expected and observed. The net result is that the time constant ( $\tau$ ) can be used to identify the cooling velocity for the cell.

The present analysis (section 2) provides a more complete evaluation of the temperature decay process such that elevated ambient temperature ( $T_a$ ) effects ( $T_{a[\text{measurement}] > T_{a[\text{calibration}]}$ ) can be accurately addressed. These analytical considerations are directly supported by experiments (section 3). The possible effects of free stream turbulence and of radiation are experimentally and inferentially addressed in section 4.

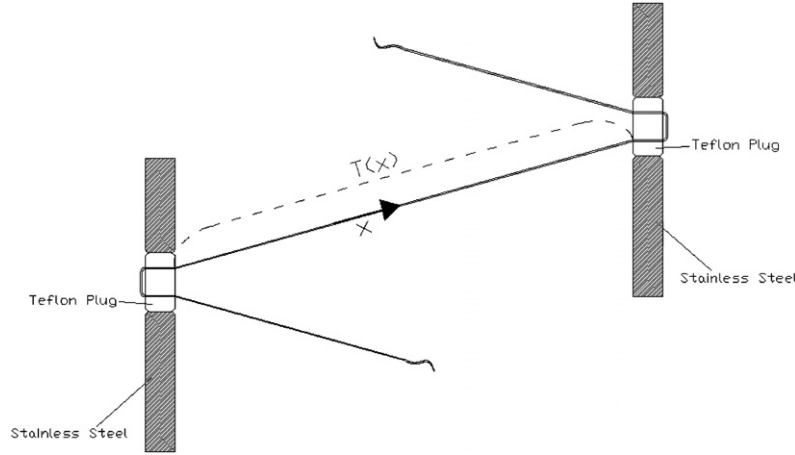
## 2. Analytical considerations

Figure 2 shows a schematic representation of a single segment of the TTA sensor wire that is secured at its two ends in the Teflon plugs which insulate the sensor wire from the electrical and thermal effects of the stainless steel frame. This figure also presents a representation of the temperature distribution in the sensor wire. The ‘flat’ central section with the ‘steep’ descent to the tether plug temperature has not been calculated. However, it is a rational representation of the sensor temperature distribution for this  $L/d \gtrsim 1000$  condition given the detailed calculations that were executed for a hot-wire sensor whose smaller ( $L/d = 200$ ) length showed a ‘flat’ central section for the velocity range of interest here [2]. Also, note that the present analysis does not rely on the specific features of  $T(x)$ .

The symbol  $T_w$  is introduced as the average temperature of the sensor wire.  $T_w$  is operationally defined by inserting the sensor’s resistance ( $R$ ) into (1) and solving for the temperature. This operationally defined average temperature will be used in the following heat transfer analysis. The analysis will be empirically tested by comparing its predictions with the data derived from the performance of the TTA system.

For  $m =$  mass of the sensor wire and  $c =$  specific heat of the sensor wire, the loss rate of thermal energy ( $\dot{Q}$ ) during the temperature decay is

$$\dot{Q} = mc \frac{dT_w}{dt}. \quad (2)$$



**Figure 2.** A segment of a TTA cell and the hypothesized/associated temperature distribution.

Standard heat transfer considerations, for example Incropera and DeWitt [3], allow  $\dot{Q}$  to be written as the sum of convective and conductive effects. Specifically,

$$\text{conduction: } -k_w A_c \left. \frac{dT}{dx} \right|_{x=0, L} \quad (3) \quad \text{or}$$

and

$$\text{convection: } -h A_p (T_w - T_a). \quad (4)$$

Here, the sign convention is ‘thermodynamic’ with thermal energy transferred from the sensor wire as a negative quantity.  $A_c$  is the cross-sectional area of the sensor wire and  $A_p$  is the perimeter area. The use of  $T_w$  (as the average temperature) in (4) is recognized to be a simplification since the central region temperatures will exceed  $T_w$  and the end regions will fall below  $T_w$ . A further modelling assumption is introduced such that the conduction term is stated to be of the form

$$\left. \frac{dT}{dx} \right|_{x=0, L} = \lambda \left\{ \frac{T_w - T_a}{d} \right\} \quad (5)$$

and it will be assumed that the scaling factor  $\lambda$  is independent from the  $T_w$  value.

The convective coefficient,  $h$ , will be modelled in terms of the Nusselt number ( $Nu$ ) where

$$Nu = \frac{hd}{k_f} \quad (6)$$

and  $k_f$  is the thermal conductivity of the air at the film temperature:

$$T_f = \left\{ \frac{T_w + T_a}{2} \right\} \quad (7a)$$

The film temperature will be further simplified for this transient condition. Namely, the maximum temperature,  $T_{\text{Hot}}$ , will be known and the single value of  $T_f$  will be arbitrarily (to be tested empirically) set to

$$T_f = \frac{T_{\text{Hot}} - 0.2(T_{\text{Hot}} - T_{\text{Low}}) + T_a}{2} \quad (7b)$$

where  $T_{\text{Low}}$  is the lowest temperature in the decay process that is used to evaluate  $\tau$ :

$$T_{\text{Low}} = T_a + 0.6(T_{\text{Hot}} - T_a). \quad (7c)$$

Modelling considerations (again, to be tested against empirical performance) suggest that, for some calibration constant  $B'$ ,

$$Nu = B'(Re^n)$$

$$\begin{aligned} h &= B' \frac{k_f}{d} \left[ \frac{Vd}{\nu_f} \right]^n \\ &= B' \frac{k_f}{\nu_f^n} (d^{n-1}) V^n. \end{aligned} \quad (8)$$

Combining (2), (5) and (8) and introducing  $A', B$  as constants,

$$\frac{1}{(T_w - T_a)} \frac{d}{dt} (T_w - T_a) = - \left\{ B \frac{k_f}{\nu_f^n} V^n + A' k_w \right\} \quad (9)$$

which leads to the final form of the predicted response equation:

$$\frac{T_w(t) - T_a}{T_w - T_a} = \exp(-t/\tau) \quad (10a)$$

where

$$\frac{1}{\tau} = \left\{ A \frac{k_w(T_a)_{\text{measurement}}}{k_w(T_a)_{\text{calibration}}} + B \frac{k_f}{\nu_f^n} V^n \right\}. \quad (10b)$$

The ‘test’ of the numerous assumptions is that  $T_w(t)$  will exhibit an exponential decay as expressed by (10a) and that it can be reliably linked to the velocity as represented by (10b).

The  $k_w$  ratio in the conduction term is to account for the ambient temperature effect on the conduction heat loss from the sensor to the tether plugs. That is, the tungsten’s thermal conductivity at an elevated ambient temperature (cf the  $k_w$  value at the calibration temperature) is addressed by this ratio.

### 3. Experimental investigation

#### 3.1. Elevated temperature flow system

A flow system that was capable of exposing a tungsten wire to elevated temperatures of 50, 70 and 100 °C at controlled velocities between 1.4 and 15 m s<sup>-1</sup> is shown in figure 3. The centrifugal blower provided a recirculating flow and the continuously operating heaters, combined with the insulation that covered the return channel and the outer housing, were

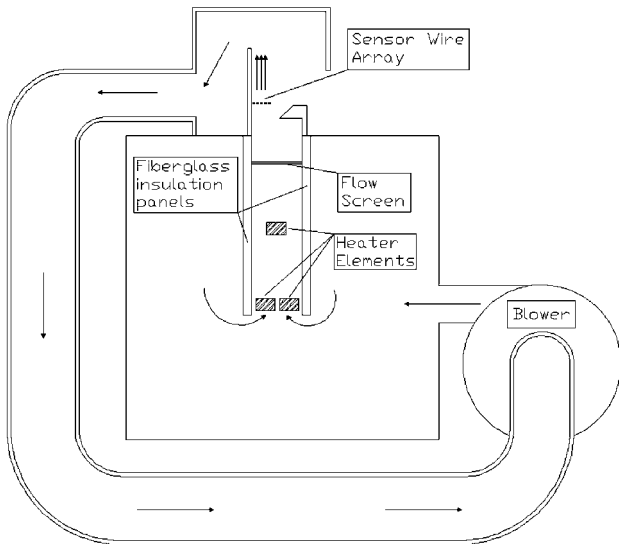


**Figure 3.** Elevated temperature flow system.

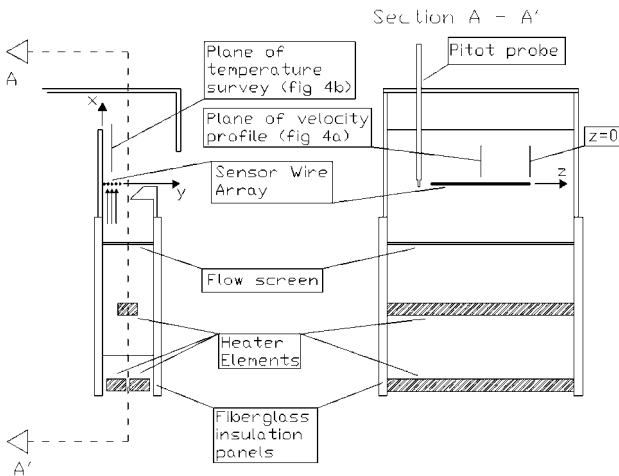


**Figure 4.** Section view at the test section to show the one-half slit-jet, the wire loops and the re-ingestion flow passage.

able to deliver an elevated temperature air stream past the sensor wire array. A detailed view of the test section (see figure 4) shows the delivery passage (formed as one-half of a slit-jet flow; see Foss and Korschelt [4] for a reference to this flow field) and the collection hood that redirects the heated air through the pressurizing blower and past the electrical heater strips. The single strand of tungsten wire was supported at tether points on insulated ‘posts’. The looped wire made ten ‘passes’ through the airflow stream for the larger diameter (0.1778 mm)<sup>2</sup> wire. The sensor wire was operated with the standard TTA electronics; see Foss *et al* [1].

The slit-jet geometry provides a spatially uniform velocity field between the outer shear layer and the inner boundary layer. Similarly, the air temperature was adequately uniform ( $\pm 2.5$  °C) in this region. Figures 5(a) and (b) provide the supporting data for the velocity and temperature distributions.

<sup>2</sup> The sensor wire was prepared by a drawing process. Hence, its diameter in the standard English sizes, 0.005 and 0.007 in, was accurately known. Hence a four-place designation given for the mm specification of the diameter.

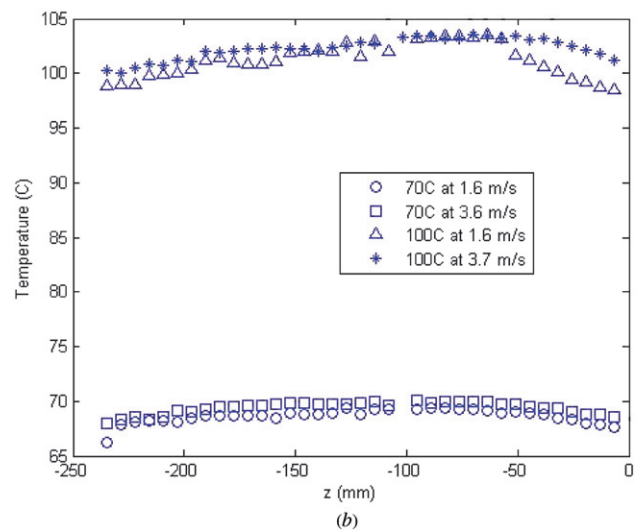
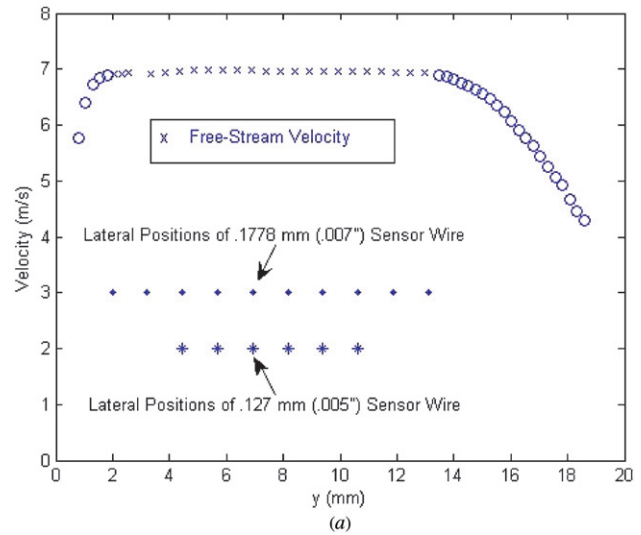


**Figure 5.** Velocity and temperature distributions at the plane of the ‘looped’ sensor wire. (a) Velocity distribution at mid-span of the test section; (b) temperature distribution across the span of the test section.

### 3.2. Experimental protocol

The recirculating air and the insulated flow system led to an elevated temperature of 30 °C without heat addition by the heater elements. Hence, 30 °C was utilized as the basic calibration condition ( $T_{a,calibration}$ ). The baseline calibration was obtained for  $1.4 \leq V \text{ (m s}^{-1}\text{)} \leq 13$ .

Power dissipation in the heaters was then used to elevate the temperature of the recirculating air. (Nominally 1 hour was required to obtain a steady state temperature for each of the target temperatures. In addition, the power input to the heaters had to be separately adjusted for each flow speed). A set of velocity values was obtained at a given temperature and the temperature was again elevated to a new target level until the data at the three elevated temperature levels were obtained.

### 3.3. Calibration results

This procedure led to an extensive body of calibration data. The aggregate information is shown in figure 6.

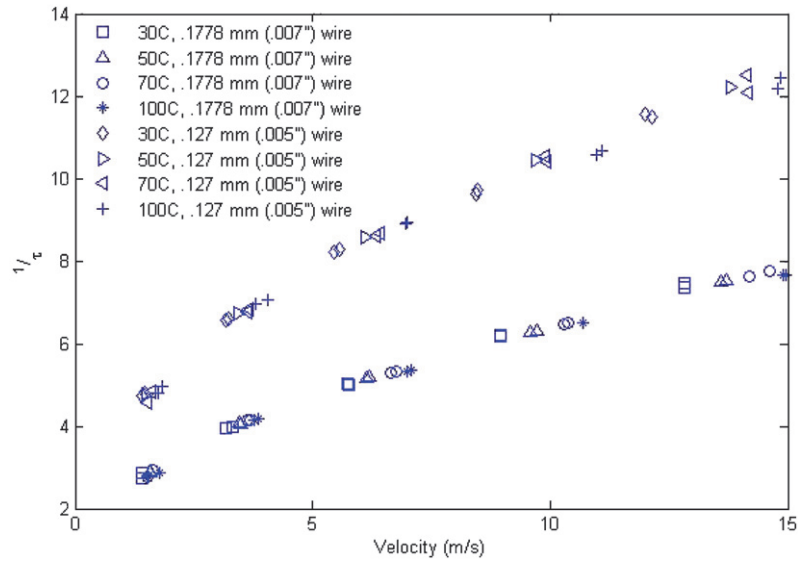


Figure 6. The complete calibration data set  $1/\tau = f(V; T_a)$ .

Equation (10b) provides a structure in which the multi-variable data of figure 6 can be brought to a compact form with the ‘correct’ selection of the exponent ‘ $n$ ’. Figure 7 presents the complete data set using the parameters of (10b) and the ‘best fit  $n$  value’ of 0.50.

The ‘best fit’ was determined by evaluating the standard deviation of the difference between the measured and the computed velocities. The latter were based upon (10b) at the 30 °C baseline condition and the use of tabulated values for  $k_w(T)$ ,  $k_f(T)$  and  $\nu_f(T)$ ; see [5, 6] respectively for the tungsten and air properties.

### 3.4. Interpretation of the results

The modelling assumptions of section 2 are considered to be well supported by the results presented in figure 7. It is not possible to individually examine these assumptions; however, the velocity and temperature ranges encompass the expected operating parameters. Hence, the data of figure 7 give confidence that the room temperature calibration can be used to adequately measure velocity magnitudes at the elevated temperatures expected in automotive as well as other, less demanding, applications.

The slopes and the intercepts of figures 7(a) and (b) are distinctly different. This is a result of absorbing the length and diameter information into the coefficients  $A$  and  $B$ . Specifically, if  $m$  in (2) were written as  $(\rho_w L A_c)$ , the conduction term of (9) would include  $L$  in the denominator and the convection term (of (9)) would contain  $d$  in its denominator. The larger slope of figure 7(a) and the smaller intercept of figure 7(b) show the effects of these geometric differences.

Since each TTA cell is individually calibrated (similar to the standard practice for hot-wire anemometry), these geometric effects need not be explicitly incorporated into (10b).

The standard deviation between the relationship of equation (10b) and the individual data points at a given  $T_a$  value provides an instructive indication of the measurement uncertainty when  $T_{a[\text{measurement}]} \neq T_{a[\text{calibration}]}$ . The  $A$ ,  $B$ ,  $n$

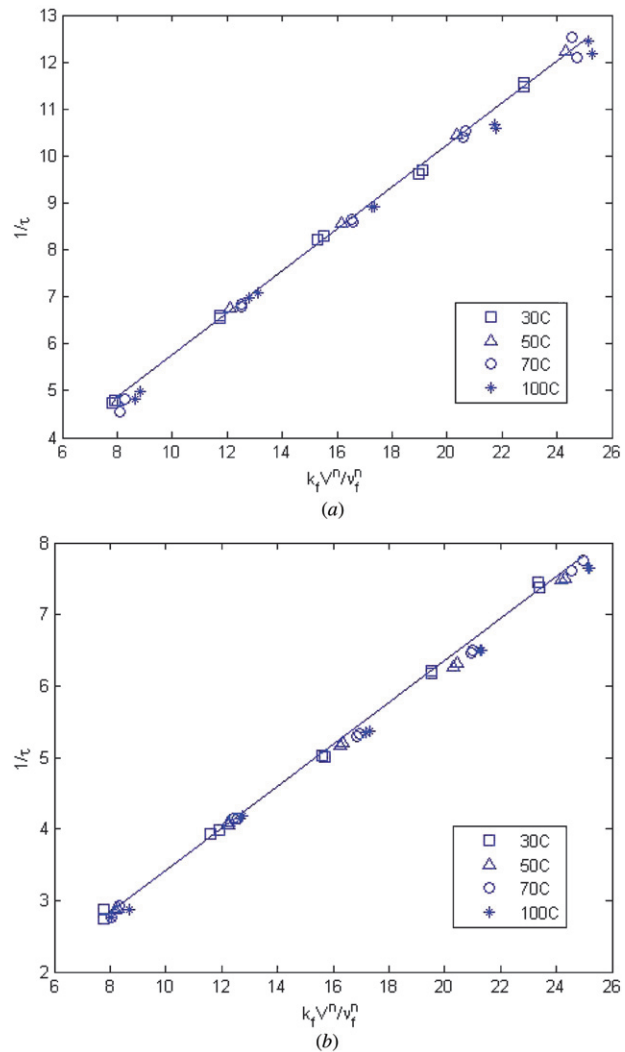
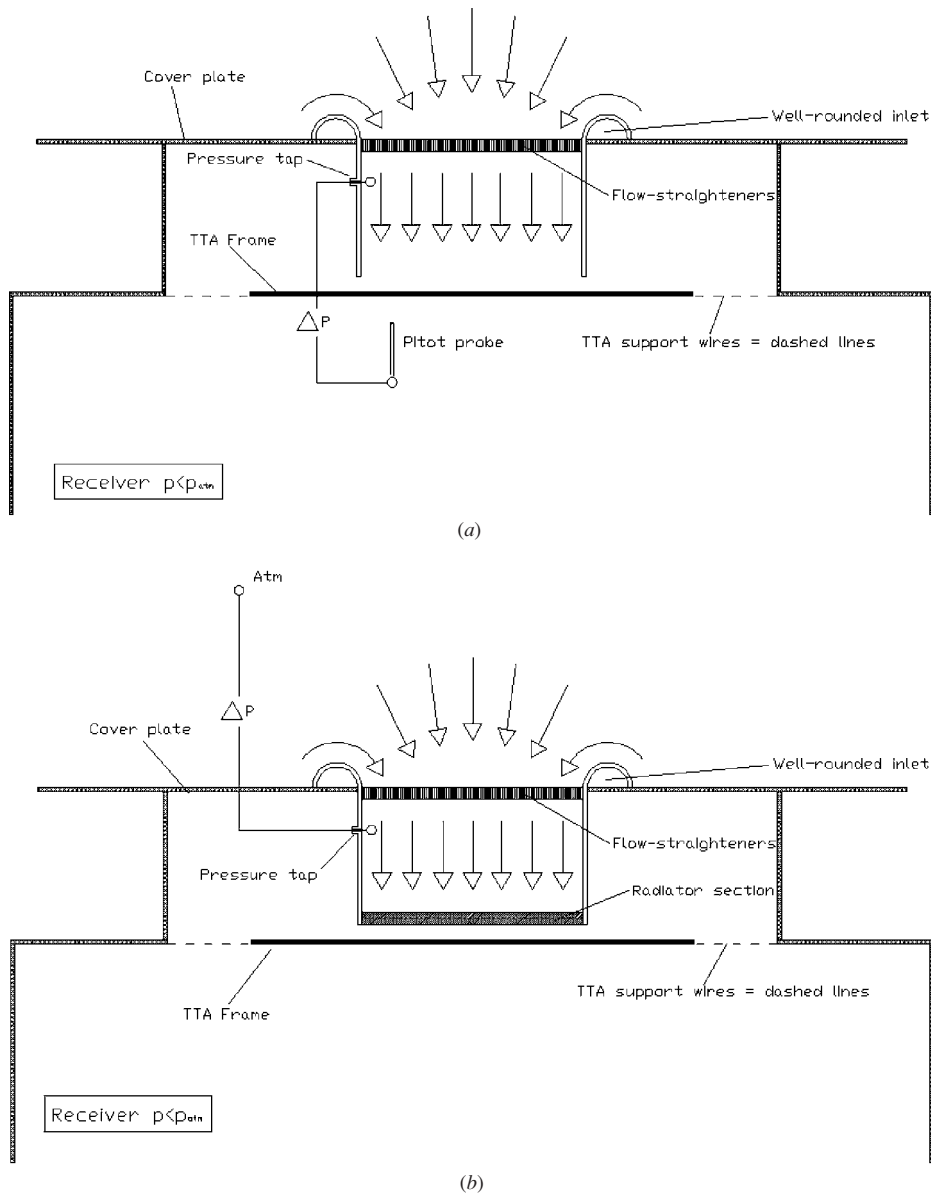


Figure 7. The complete calibration data set in the coordinates suggested by (10b) with  $n = 0.50$ . (a) Sensor diameter = 0.127 mm (0.005''); (b) sensor diameter = 0.1778 mm (0.007'').



**Figure 8.** Low disturbance/elevated disturbance calibration flow delivery conduit. (a) Low disturbance condition; (b) elevated disturbance condition.

**Table 1.** Standard deviation values.

Sensor wire	$T =$	50 °C	70 °C	100 °C
$d = 0.128 \text{ mm}$ (reference condition $\sigma(T_{\text{cal}}) = 0.17 \text{ m s}^{-1}$ )	$\sigma(T_a \neq T_{\text{cal}}) \text{ m s}^{-1}$	0.57	0.58	0.33
$D = 0.1778 \text{ mm}$ (reference condition $\sigma(T_{\text{cal}}) = 0.17 \text{ m s}^{-1}$ )	$\sigma(T_a \neq T_{\text{cal}}) \text{ m s}^{-1}$	0.23	0.18	0.11

$$\sigma = \left\{ \frac{1}{N-1} \sum_{j=1}^N [V_{\text{calc}} - V_{\text{meas}}]_j^2 \right\}^{1/2} \quad (11)$$

The  $V_{\text{calc}}$  value is defined using the measured  $\tau$  value for a given  $j$ th sample.

It is noteworthy that these  $\sigma$  values are quite adequate to guide the cooling air circuit developments for a typical automotive application.

#### 4. Free stream turbulence and radiation effects

##### 4.1. Free stream turbulence

The calibration airstream for evaluating the  $1/\tau = f(V)$  response of a TTA cell is most easily provided with a low (i.e., a controlled) free stream turbulence level. Applications that can

values of (10b) are established by the calibration data at 30 °C. Hence, the standard deviation at 30 °C establishes the minimum uncertainty for the TTA readings.

Table 1 provides the relevant standard deviation ( $\sigma$ ) values. Note that  $\sigma$  is defined as

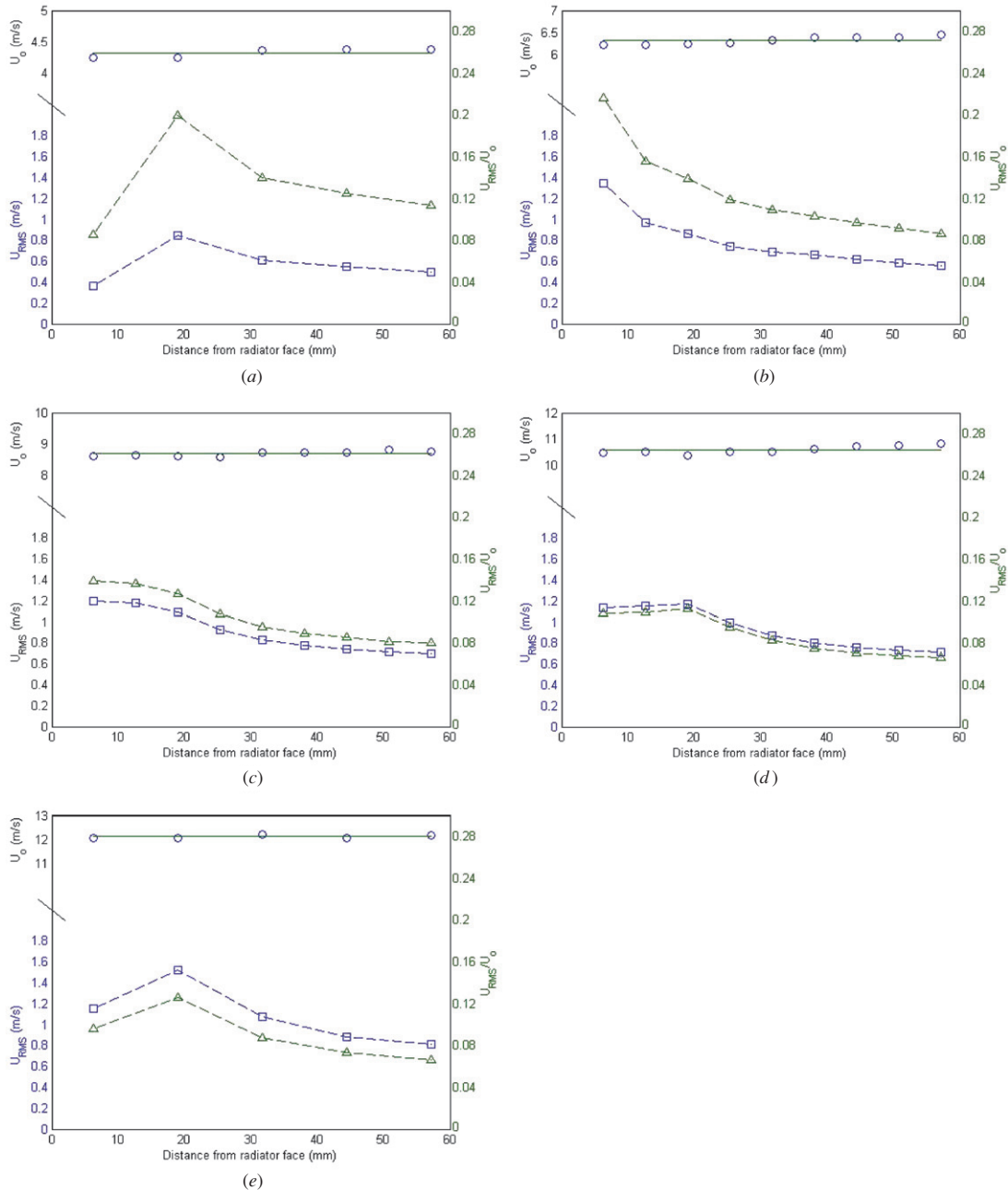


**Figure 9.** Evaluation of the TTA response to varying free stream turbulence levels. *Notes:* (i) wire diameter = 0.1778 mm (0.007"); (ii) velocity recorded by the TTA,  $u_o(\circ)$ , fluctuation intensity,  $\tilde{u}(\square)$ , relative intensity,  $\tilde{u}/u_o(\triangle)$ ; (iii) connecting dashed lines for visual reference only; (iv) average velocity,  $\langle V \rangle$ , obtained from TTA and shown as the solid line, (a) Average  $V = 4.32 \text{ m s}^{-1}$ , (b) average  $V = 6.33 \text{ m s}^{-1}$ , (c) average  $V = 8.69 \text{ m s}^{-1}$ , (d) average  $V = 10.59 \text{ m s}^{-1}$ , (e) average  $V = 12.13 \text{ m s}^{-1}$ ; (v) 95% confidence bound ( $2\sigma$ ) =  $0.34 \text{ m s}^{-1}$  for the  $\langle V \rangle$  values.

involve elevated disturbance levels must be considered if the TTA is to be considered to be a ‘universal’ instrument. Hence, experiments were conducted in which a low disturbance stream was disturbed by a section of a ‘sacrificed’ radiator.

This calibration environment is shown in figure 8. ‘Flow-straighteners’ comprising a honeycomb/screen assembly were used to provide a low disturbance environment for the calibration flow, as shown in figure 8(a). The data of figures 6 and 7 were obtained with this configuration. The configuration of figure 8(a) was calibrated such that  $(p_{atm} - p_{tap})$  could be used to specify the uniform velocity distribution at the TTA

cell. Figure 8(a) shows the direct measurement of velocity given the  $\Delta p = p_{Pitot} - p_{tap}$  value. At this flow rate, the tap is then connected differentially to the atmosphere to provide

$$V = f[p_{atm} - p_{tap}]. \quad (12)$$

When the sacrificed radiator is installed, the calibration function of (12) is used to determine  $V$ , as shown in figure 8(b).

A single cell of a TTA frame was calibrated in the low disturbance environment. It was then placed at a series of downstream distances from the radiator segment.

Concurrently, a single hot-wire probe was moved in the streamwise direction with the TTA frame. (It is recognized that the hot wire provides a ‘single point sample in an inhomogeneous turbulence field’. This realization is the motivation for the long length of the TTA sensor wire). The principal function of the hot-wire probe is to provide an indication of the turbulence intensity value.

Figures 9(a)–(e) present the results from this evaluation of the flow disturbance effects. The evident ‘message’ is that the TTA output is quite insensitive to the disturbance level of the approach flow. It is not claimed that the hot-wire values of  $\bar{u}$  (fluctuation intensity) are representative of an area average since the measurement is over a length of 1 mm. However, the trend of decreasing  $\bar{u}$  downstream of the second measurement location is compatible with the expected decay of the turbulence kinetic energy downstream of the sacrificed radiator. Since the basic calibration for the cell was carried out in a low disturbance environment, the insensitivity to  $\bar{u}$  is considered to be established.

#### 4.2. Radiation effects

The heat transfer model leading to (10b) does not include radiation. Specifically, it only involves the temperature difference between the ambient and the sensor wire.

Since radiation is represented by the difference of  $T^4$  values (sensor-to-surroundings), the exponential relationship could not describe the heat transfer effects at strongly different absolute temperatures for the same temperature differences. Hence, the observed success of (10a) to fit the observations with  $T_a = 30, 50, 70$  and  $100$  °C is accepted as a conclusive statement that radiation does not influence the heat transfer effects of the TTA.

## 5. Summary and conclusions

The basic attributes of the thermal transient anemometer (TTA) which provide area averaged velocity and temperature values over a cell (of a TTA frame) were introduced by Foss *et al* [1]. A laboratory ambient temperature calibration is used to establish the relationship

$$\frac{1}{\tau} = A + B\langle V^n \rangle, \quad (13)$$

whereby the decay time constant of the sensor wire ( $T_{\text{Hot}} \rightarrow T_{\text{Low}}$ ), following the cessation of the heating current, can be used to infer the area average velocity ( $\langle V \rangle$ ) at the cell.

The analytical considerations to extrapolate this transfer function to other ambient temperature values has been given (see (10b)) and confirmed by the present experiments.

In addition, it has been empirically demonstrated that practical levels of free stream turbulence and heat transfer by radiation do not influence the  $1/\tau \sim \langle V \rangle$  relationship.

## References

- [1] Foss J F, Schwannecke J K, Lawrenz A R, Mets M W, Treat S C and Dusel M D 2004 The thermal transient anemometer *Meas. Sci. Technol.* **15** 2248–55
- [2] Morris S C and Foss J F 2003 Transient thermal response of a hot-wire anemometer *Meas. Sci. Technol.* **14** 251–9
- [3] Incropera F P and DeWitt D P 1981 *Fundamental of Heat Transfer* (New York: Wiley)
- [4] Foss J F and Korschelt D 1983 Instabilities in the slit-jet flow field *J. Fluid Mech.* **132** 79–86
- [5] Weast R E 1970 *Handbook of Chemistry and Physics* 51st edn (Boca Raton, FL: CRC Press)
- [6] Johnson R W 1998 *The Handbook of Fluid Dynamics* (Boca Raton, FL: CRC Press)